Title

Mode of Surgical Injury Influences the Source of Urothelial Progenitors during Bladder Defect Repair

Journal

Stem Cell Reports, 9(6)

ISSN

2213-6711

Authors

Schäfer, Frank-Mattias
Algarrahi, Khalid
Savarino, Alyssa
et al.

Publication Date

2017-12-01

DOI

10.1016/j.stemcr.2017.10.025

Peer reviewed

Stem Cell Reports
Article

OPEN ACCESS

Mode of Surgical Injury Influences the Source of Urothelial Progenitors during Bladder Defect Repair

Frank-Mattias Schäfer,[1,2] Khalid Algarrahi,[1,2] Alyssa Savarino,[1,2] Xuehui Yang,[1,2] Catherine Seager,[1,2] Debra Franck,[1,2] Kyle Costa,[1,2] Shanshan Liu,[3] Tanya Logvinenko,[1,2,3] Rosalyn Adam,[1,2] and Joshua R. Mauney[1,2,*]

[1]Urological Diseases Research Center, Boston Children's Hospital, Boston, MA 02115, USA
[2]Department of Surgery, Harvard Medical School, Boston, MA 02115, USA
[3]Institutional Centers of Clinical and Translational Research, Boston Children's Hospital, Boston, MA 02115, USA
*Correspondence: joshua.mauney@childrens.harvard.edu
https://doi.org/10.1016/j.stemcr.2017.10.025

SUMMARY

The bladder urothelium functions as a urine-blood barrier and consists of basal, intermediate, and superficial cell populations. Reconstructive procedures such as augmentation cystoplasty and focal mucosal resection involve localized surgical damage to the bladder wall whereby focal segments of the urothelium and underlying submucosa are respectively removed or replaced and regeneration ensues. We demonstrate using lineage-tracing systems that urothelial regeneration following augmentation cystoplasty with acellular grafts exclusively depends on host keratin 5-expressing basal cells to repopulate all lineages of the *de novo* urothelium at implant sites. Conversely, repair of focal mucosal defects not only employs this mechanism, but in parallel host intermediate cell daughters expressing uroplakin 2 give rise to themselves and are also contributors to superficial cells in neotissues. These results highlight the diversity of urothelial regenerative responses to surgical injury and may lead to advancements in bladder tissue engineering approaches.

INTRODUCTION

The bladder urothelium is a transitional epithelium that serves as a urine-blood barrier and consists of basal, intermediate, and superficial cells (Wu et al., 2009). Normally quiescent, the urothelium undergoes rapid cell division and differentiation to restore barrier function within defect sites (Khandelwal et al., 2009), a process mediated by urothelial progenitors. Recent lineage-tracing experiments of urothelial regeneration in chemical- or bacterial-induced injury models have demonstrated that the sonic hedgehog (SHH)-expressing population, which includes basal and intermediate cells, contains progenitor populations (Shin et al., 2011; Gandhi et al., 2013; Papafotiou et al., 2016). However, controversy over cellular lineage hierarchy exists, and both linear and nonlinear models of urothelial regeneration from SHH$^+$ progenitors have been proposed. In particular, a study from Gandhi and colleagues reported that urothelial regeneration in adult mice is mediated by independent basal and intermediate cell progenitors that form *de novo* basal and superficial cell layers along distinct pathways, thus supporting a nonlinear progression (Gandhi et al., 2013). In contrast, a report from Papafotiou et al. (2016) recently provided evidence for a linear regenerative sequence in which basal cells as well as a keratin 14 (KRT14)-positive basal subpopulation could serve as precursors for all three *de novo* layers in adult mice following bladder injury. It is currently unknown whether these models are mutually exclusive, and it remains poorly understood how the nature of urothelial injury influences subsequent regenerative responses.

Surgical management of the urinary bladder is frequently indicated in both benign and malignant bladder disorders. Augmentation cystoplasty with autologous gastrointestinal segments or acellular biomaterials have been performed to increase bladder capacity, reduce urinary storage pressures, and preserve renal function in patients afflicted with benign urologic diseases such as bladder outlet obstruction (Veeratterapillay et al., 2013; Schaefer et al., 2013; Zhang and Liao, 2014). For malignant conditions, transurethral bladder resection is often utilized to stage bladder cancer as well as remove nonmuscle invasive cancerous lesions from the bladder (Richards et al., 2014). Both transurethral bladder resection and augmentation cystoplasty with biomaterials involve localized surgical injury to the bladder wall whereby focal segments of the urothelium and underlying submucosa are respectively removed or replaced and regeneration ensues. These modes of injury differ from chemical and microbial insults, which primarily result in exfoliation of superficial cells while leaving underlying urothelial subpopulations intact (Mysorekar et al., 2009; Gandhi et al., 2013; Abraham and Miao, 2015). The identity and lineage hierarchy of urothelial progenitors during constructive remodeling of surgical defects is largely unknown.

In the current study, we show that the type of surgical bladder damage dictates the manner in which urothelial repair processes occur. Specifically, we demonstrate using fate-mapping systems that urothelial regeneration at

acellular graft sites primarily depends on host basal cell progeny to repopulate all lineages of the *de novo* urothelium in a sequential fashion. On the other hand, healing of focal mucosal defects created by bladder resection not only employs this mechanism, but in parallel, host intermediate cell daughters give rise to themselves and are also a source of superficial cells in neotissues. These findings shed light on the diversity of urothelial regenerative responses to surgical injury and show that both the linear and nonlinear regenerative models can occur concurrently in response to particular types of injury. These results may have important implications for urologic tissue engineering applications.

RESULTS

Characterization of Steady-State Adult Murine Urothelium

Basal, intermediate, and superficial cell populations of the adult murine urothelium have been previously characterized by their location, size, and expression of molecular markers (Gandhi et al., 2013; Balsara and Li, 2017; Kullmann et al., 2017). Superficial cells comprise the apical layer of the urothelium and range between 40 and 250 μm in diameter depending on the level of bladder distension (Kullmann et al., 2017). This cell population has been reported to express uroplakins and KRT20 while lacking markers such as SHH, tumor promoter p53-like family member TP63 (P63), and KRT5 (Kullmann et al., 2017). Intermediate cells underlie superficial cells and are significantly smaller in diameter (~10–20 μm) (Balsara and Li, 2017; Kullmann et al., 2017). Gandhi et al. (2013) distinguished intermediate cells from superficial cells by their expression of P63 and SHH (Gandhi et al., 2013), while Kullmann et al. (2017) noted that KRT20 expression is absent in the intermediate cell population. Finally, $KRT5^+$ basal cells are positioned along the basement membrane and constitute the most abundant cell population in the adult urothelium (Gandhi et al., 2013). This population can be identified by SHH and P63 positivity coupled with the absence of UP and KRT20 markers (Gandhi et al., 2013; Kullmann et al., 2017). Based on these previous characterizations (Gandhi et al., 2013; Balsara and Li, 2017; Kullmann et al., 2017), we performed KRT5, P63, UP, and KRT20 immunolabeling of bladder specimens described in this study to discriminate urothelial subpopulations. We observed that the urothelium of the adult mouse bladder under steady-state conditions is composed of $KRT5^+P63^+UP^-KRT20^-$ basal (BC-1) cells, 1–2 layers of $KRT5^-P63^+UP^+KRT20^-$ intermediate (IC-1) cells, and a luminal layer of $KRT5^-P63^-UP^+KRT20^+$ superficial (S) cells (Figures 2 and 3).

Characterization of Urothelial Regenerative Stages following Bladder Augmentation

Augmentation cystoplasty was performed with small intestinal submucosa (SIS) scaffolds in wild-type (WT) mice. This surgical procedure creates a full-thickness defect in the bladder wall, which is repaired by anastomosis of an SIS graft to the surrounding host tissue in order to seal the lumen (Figure 1A). Reconstructed bladders were subjected to histological, immunohistochemical (IHC), and histomorphometric analyses over the course of 8 weeks to characterize the various stages of urothelial regeneration at implant sites (Figure 2). In parallel, regions of the bladder wall that were not replaced by SIS grafts were analyzed as internal nonaugmented controls (NAC), while unoperated bladders served as nonsurgical controls (NSC).

At 2 weeks postoperatively (post-op), SIS matrices had undergone substantial degradation, and a fibrovascular scar populated with fibroblasts as well as inflammatory mononuclear cells was apparent throughout the original graft region. No smooth muscle regeneration was observed in the remodeling bladder wall at this time point. A hyperplastic urothelium was present at the peripheral borders of the implant site and contained proliferating $Ki67^+$ cells, which constituted 33% ± 5% of the $KRT5^+$ cell compartment. In addition, two previously unreported urothelial subpopulations, $KRT5^+P63^-UP^-KRT20^-$ (BC-2 cells) and $KRT5^-P63^-UP^+KRT20^-$ (IC-2 cells), were observed along the implant perimeter, but were not present in NSC bladders and only rarely observed in NAC fields. In neotissues, BC-2 cells were found to represent 14% ± 7% of the total $KRT5^+$ cell population while IC-2 cells comprised 92% ± 6% of the total UP^+ population, with the remainder populations displaying classical BC-1 and IC-1 phenotypes, respectively. At the interface between the $KRT5^+$ and UP^+ cell layers, BC-2 cells were observed protruding into the predominantly IC-2 layer and displayed overlapping expression of UP, suggestive of IC-2 differentiation. No S cells were observed in the implant region at this phase of wound healing.

By 4 weeks post repair, fibrosis was evident in the neobladder wall and inflammatory cell infiltrates persisted throughout the remodeling tissue. At this stage the *de novo* urothelium was still hyperplastic, but now lined the entire graft region. In neotissues, the IC-2 population had significantly declined from 2-week levels to 67% ± 9% of the total UP^+ cell population while the proportion of IC-1 cells was significantly elevated by ~4-fold in respect of 2-week values. The increase in the IC-1 population correlated with areas of BC-1 cells extending from the $KRT5^+$ cell compartment and coexpressing UP, consistent with the notion that they may be precursors of the IC-1 population. No evidence of activated caspase-3 staining was observed in IC-2 cells; however, shed clusters of this cell

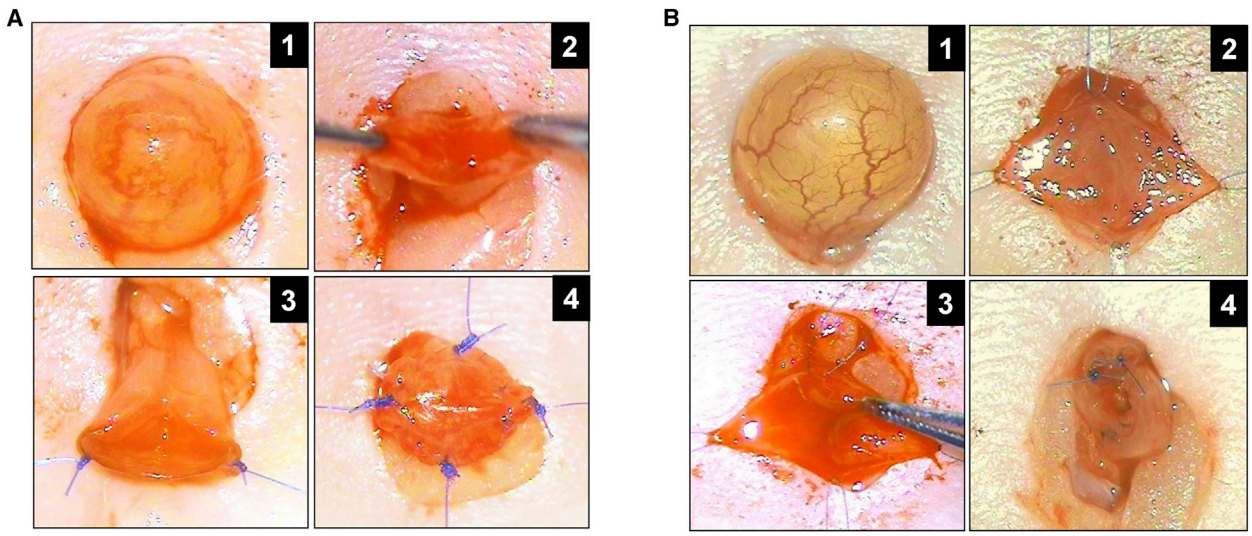

Figure 1. Surgical Bladder Injury Models in Mice

(A) Augmentation cystoplasty with SIS graft. Panel 1: exposure of bladder prior to scaffold implantation. Panel 2: cystotomy and exposure of bladder lumen. Panels 3 and 4: anastomosis of graft into bladder defect and placement of marking sutures.

(B) Focal resection of bladder mucosa. Panel 1: bladder exposure prior to surgical injury. Panel 2: midline incision of bladder wall. Panel 3: resection of bladder mucosa from one hemisphere of the bladder. Panel 4: bladder closure and integration of marking sutures at defect site perimeter.

See also Figure S1.

type were routinely detected in the bladder lumen, indicating that exfoliation rather than an apoptotic event may be responsible for the decline in this population. BC-1 and BC-2 cells were present in similar proportions as detected at the 2-week time point; however, the incidence of Ki67 positivity in the $KRT5^+$ cell compartment had markedly diminished. In addition, S cells were occasionally observed in the implant site at 4 weeks post-op but constituted only 1% of the UP^+ population present. Histomorphometric evaluations of NAC regions at 4 weeks post repair revealed similar levels of all urothelial subpopulations as observed in NSC controls, suggesting that urothelial regenerative processes were localized to the graft site alone.

Following 8 weeks of scaffold implantation, the morphology of the urothelium in neotissues resembled NSC and NAC regions and consisted of BC-1, IC-1, and S cell populations, while BC-2 and IC-2 subpopulations were largely undetectable. Moreover, no significant differences were detected in the percentages of each urothelial subpopulation present in neotissues in comparison with the respective NAC regions and NSC specimens, suggesting that the regenerative process in the urothelium had resolved. These results reveal that bladder reconstruction with SIS grafts promotes urothelial repair mechanisms involving transitory BC-2 and IC-2 populations, and demonstrates that formation of BC-1, IC-1, and S cell types occurs in a temporal fashion at implant sites. In contrast, the neobladder wall at this time point contained extensive fibrosis and inflammatory cell infiltrates with only islands of nascent smooth muscle bundles observed. These data are consistent with our previous studies demonstrating that SIS grafts lead to an immature state of bladder wall repair in a murine bladder augmentation model (Mauney et al., 2011).

Characterization of Urothelial Regenerative Stages following Focal Mucosal Resection

Focal resection of bladder mucosa was performed in WT mice. This injury model creates a partial-thickness bladder defect by resecting the urothelium and underlying mucosa from two-thirds of the luminal surface area following cystotomy (Figure 1B). Histological, IHC, and histomorphometric evaluations were performed on reconstructed bladders 12 hr following resection to characterize the initial injury site (Figure S1) and over the course of 3 weeks of repair to determine the phases of urothelial regeneration (Figure 3). In addition, nonresected control (NRC) regions of the bladder wall from operated animals were analyzed in parallel as internal standards in combination with NSC specimens.

Twelve hours after focal mucosal resection, we confirmed that the host urothelium was completely removed from the defect region, since no $KRT5^+$ or UP^+ urothelial

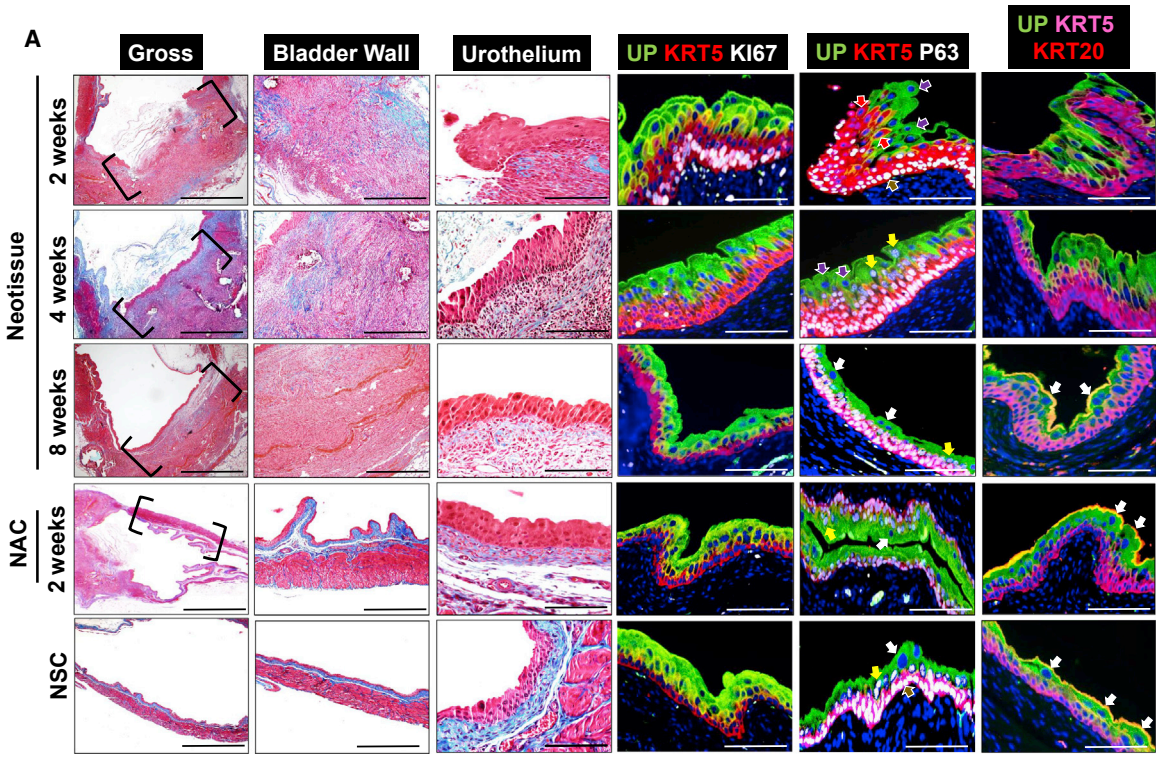

B

% of total KRT5+ population ± S.D.							
	NSC	Neotissue			NAC		
	0 weeks	2 weeks	4 weeks	8 weeks	2 weeks	4 weeks	8 weeks
BC-1	100±0	86±7	83±8	97±3	99±1	99±1	99±1
BC-2	0±0	14±7	17±8	3±3	1±1	0.3±0.6	0.3±1
% of total UP+ population ± S.D.							
	NSC	Neotissue			NAC		
	0 weeks	2 weeks	4 weeks	8 weeks	2 weeks	4 weeks	8 weeks
IC-1	83±6	8±6	33±8*	83±6*	72±1	85±4	85±5
IC-2	0±0	92±6	67±9*	0±0*	0±0	0±0	0±0
S	17±6	0±0	1±0.6	17±6*	28±1	15±4	15±6

C

% of KI67+ cells in KRT5+ and UP+ populations ± S.D.							
	NSC	Neotissue			NAC		
	0 weeks	2 weeks	4 weeks	8 weeks	2 weeks	4 weeks	8 weeks
KRT5+	0.7±1	33±5	9±2	0±0	4±4	0.2±0.3	0±0
UP+	0±0	1±2	2±3	0±0	1±2	0±0	2±2

Figure 2. Stages of Urothelial Regeneration at SIS Scaffold Implantation Sites

(A) Column 1: MTS-stained gross bladder cross-sections from WT mice containing original SIS implant sites or nonaugmented control (NAC) regions (bracketed) following 2, 4, and 8 weeks post-op. Nonsurgical controls (NSC) analyzed in parallel. Column 2: magnification of bladder wall in implant or NAC regions bracketed in column 1 as well as parallel NSC. Column 3: magnification of urothelium in neotissues and NAC regions bracketed in column 1 as well as parallel regions of NSC. Columns 4–6: representative photomicrographs of tissues described in column 3 and subjected to IHC analyses for uroplakin (UP) 3A, KRT5, KI67, P63, or KRT20 protein expression. For all photomicrographs in, respective marker expression is displayed in red, green, or pink (Cy3, FITC, Cy5 labeling), and blue denotes DAPI nuclear counterstain. In columns 3 and 4, Cy5 labeling was false colored to white. Brown arrows denote BC-1 cells ($KRT5^+P63^+UP^-KRT20^-$), red arrows denote BC-2 cells ($KRT5^+P63^-UP^-KRT20^-$), yellow arrows denote IC-1 cells ($KRT5\text{-}P63^+UP^+KRT20^-$), purple arrows denote IC-2 cells

(legend continued on next page)

subpopulations were observed along the luminal perimeter of the injured bladder wall (Figure S1). In contrast, the host urothelium at the border of the defect site and in NRC regions was intact and consisted of proliferating Ki67$^+$ cells throughout the KRT5$^+$ and UP$^+$ cell compartments (Figure S1). Following 3 days post injury, invasion of the host urothelium into the periphery of the defect site had occurred with the neoepithelium consisting of BC-1, BC-2, and IC-2 cell types. At this stage, no IC-1 or S cells were detected within the defect region, in contrast to NRC regions and NSC specimens. The *de novo* urothelium was hyperplastic and proliferating Ki67$^+$ cells constituted 26% ± 9% of the KRT5$^+$ cell compartment. In addition, discrete pockets of BC-2 cells were found coexpressing UP at the border between the KRT5$^+$ and UP$^+$ cell compartments comparable with those seen following 2 weeks of SIS scaffold implantation. At this stage of repair, the remodeling bladder wall was colonized with mononuclear inflammatory cells as well as fibroblast populations, while residual smooth muscle bundles were observed in the injured site from closure of the primary defect. Edema was evident throughout the reconstructed and NRC regions of the bladder wall.

By 1 week post-op, the *de novo* urothelium extended across the original defect site and contained BC-1, BC-2, IC-1, and IC-2 cell pools. IC-1 cells had substantially increased from the 3-day time point to 55% ± 19% of the total UP$^+$ cell population while exfoliation of IC-2 cells was apparent within the bladder lumen. The mean percentage of proliferating Ki67$^+$ cells in both the KRT5$^+$ and UP$^+$ cell compartments was 5% in neotissues at this stage. In addition, BC-1 cells were observed protruding into the UP$^+$ cell compartment and demonstrated overlapping UP expression, indicative of IC-1 differentiation. S cells were rarely detected in the neoepithelium at this stage of repair. In addition, inflammatory mononuclear cells were frequently observed throughout the remodeling bladder wall at this time point.

At 3 weeks post injury, normal urothelial architecture was restored at the defect site with percentages of BC-1, IC-1, and S subpopulations similar in neotissues as compared with NSC and NRC regions. BC-2 and IC-2 were grossly absent in the neoepithelium at this stage. Inflammatory mononuclear cells had qualitatively declined in the repaired bladder wall compared with the 1-week time point while host smooth muscle bundles were primarily concentrated in the periphery of the original defect site. Similar to bladder reconstruction with acellular grafts, regeneration of mucosal defects results in a linear progression of BC-1, IC-1, and S cell formation in combination with the occurrence of transitory phenotypes, BC-2 and IC-2, albeit at a faster rate.

Validation of Transgenic Mouse Models for Lineage Tracing of Urothelial Subpopulations during Regeneration

The SHH$^+$ population of the urothelium contains BC-1 and IC-1 phenotypes, and both have been implicated as progenitor cell sources in response to chemical- and bacterial-induced injury (Shin et al., 2011; Gandhi et al., 2013), although the role they play in urothelial regeneration following various types of surgical injury is unclear. To address this question, we performed fate-mapping studies in *Krt5*^{CreERT2};mTmG and *Upk2*^{iCreERT2};mTmG mice using Cre-lox recombination to indelibly label either host KRT5$^+$ (BC-1) and UP$^+$ cell populations (IC-1, S cells), respectively as well as their associated daughters, during regeneration of SIS graft sites or mucosal defects. Prior to surgical injury, IHC analyses (Figure 4A) demonstrated that both tamoxifen (Tm)-induced NSC lines displayed >80% recombination efficiency. GFP expression was exclusively localized to KRT5$^+$ BC-1 cells in the *Krt5*^{CreERT2};mTmG strain while GFP was solely detected in UP$^+$ IC-1 and S cells in the *Upk2*^{iCreERT2};mTmG line. Parallel control animals receiving vehicle injections alone showed no evidence of recombination (data not shown).

Host KRT5$^+$ BC-1 Cells Are the Progenitor Population Responsible for *De Novo* Urothelial Formation at Bladder Augment Sites

Krt5^{CreERT2};mTmG and *Upk2*^{iCreERT2};mTmG mice were subjected to Tm induction before bladder augmentation with SIS scaffolds, and BC-1 and IC-1 cell progeny were traced in implant sites over the course of graft remodeling. At 4 weeks post-op, IHC evaluations of the implant regions in *Krt5*^{CreERT2};mTmG bladders revealed GFP expression in all urothelial lineages at this time point, including BC-1, BC-2, IC-1, and IC-2 phenotypes (Figure 4B). At 8 weeks post-op, GFP$^+$ BC-1 and IC-1 cells were apparent throughout the neotissues (Figure 4C) and, moreover,

(KRT5$^-$P63$^-$UP$^+$KRT20$^-$), and white arrows denote S cells (KRT5$^-$P63$^-$UP$^+$KRT20$^+$). Scale bars represent 1 mm (column 1), 500 μm (column 2), and 200 μm (columns 3–6).

(B) Histomorphometric evaluations of urothelial subpopulations in NSC as well as neotissues and corresponding NAC regions following 2, 4, and 8 weeks post-op. Means ± SD. *$p < 0.05$ in comparison with respective 2-week time point as determined by Wilcoxon signed-rank test.

(C) Histomorphometric evaluations of Ki67$^+$ cells in specimens described in (B). Means ± SD.

Data in all panels were acquired from n = 3–4 animals per experimental group with n = 3 sections per animal analyzed for neotissue, NAC, and NSC evaluations.

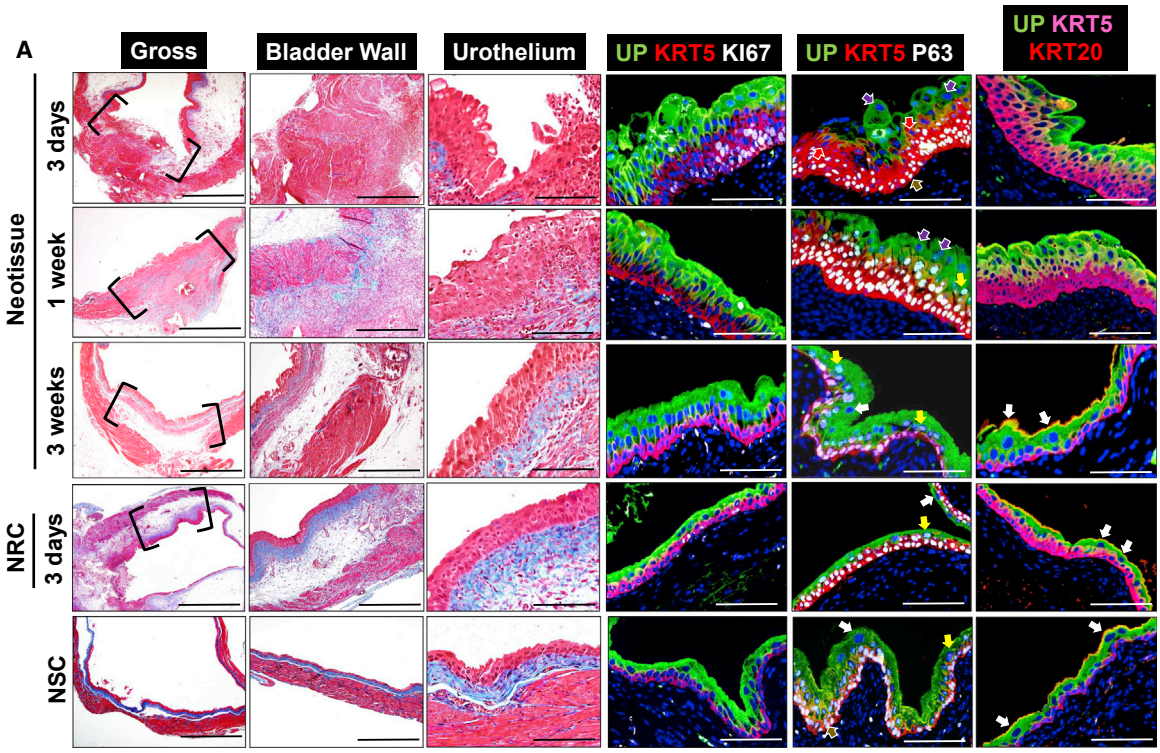

B

% of total KRT5+ population ± S.D.							
	NSC	Neotissue			NRC		
	0 weeks	3 days	1 week	3 weeks	3 days	1 week	3 weeks
BC-1	100±0	87±4	95±3	99±1	98±2	98±1	100±0
BC-2	0±0	13±4	5±3	1±1	2±2	2±1	0±0
% of total UP+ population ± S.D.							
	NSC	Neotissue			NRC		
	0 weeks	3 days	1 week	3 weeks	3 days	1 week	3 weeks
IC-1	83±6	0±0	55±19	80±2	75±11	80±9	84±5
IC-2	0±0	100±0	43±21	0±0*	0±0	0±0	0±0
S	17±6	0±0	2±2	20±2	22±14	20±9	16±5

C

% of KI67+ cells in KRT5+ and UP+ populations ± S.D.							
	NSC	Neotissue			NRC		
	0 weeks	3 days	1 week	3 weeks	2 weeks	4 weeks	8 weeks
KRT5+	0.7±1	26±9	5±3	0±0	5±2	1±2	1±2
UP+	0±0	3±3	5±2	0±0	6±6	0±0	0±0

Figure 3. Phases of Urothelial Regeneration at Regions of Focal Mucosal Resection

(A) Column 1: MTS-stained gross bladder cross-sections from WT mice containing mucosal defect sites or nonresected control (NRC) regions (bracketed) following 3 days, 1 week, and 3 weeks post-op. Nonsurgical controls (NSC) analyzed in parallel. Column 2: magnification of bladder wall in implant or NRC regions bracketed in column 1 as well as parallel NSC. Column 3: magnification of urothelium in neotissues and NRC regions bracketed in column 1 as well as parallel regions of NSC. Columns 4–6: representative photomicrographs of tissues described in column 3 and subjected to IHC analyses for uroplakin (UP) 3A, KRT5, KI67, P63, or KRT20 protein expression. For all photomicrographs, respective marker expression is displayed in red, green, or pink (Cy3, FITC, Cy5 labeling), and blue denotes DAPI nuclear counterstain. In columns 3 and 4, Cy5 labeling was false colored to white. Brown arrows denote BC-1 cells ($KRT5^{+}P63^{+}UP^{-}KRT20^{-}$), red

(legend continued on next page)

81% ± 12% of S cells displayed GFP expression (Figure 4E). Evaluation of NAC regions at this time point demonstrated that GFP expression was primarily localized to BC-1 cells and only occasionally observed in UP$^+$ populations, potentially due to BC-1 cell differentiation as a result of global surgical manipulation (Figure 4C). Parallel analysis of *Upk2*^{iCreERT2};mTmG bladders at 8 weeks post-op failed to show GFP expression in *de novo* IC-1 and S cell populations (Figures 4D and 4E), while robust GFP expression was observed in host IC-1 and S cell populations contained in NAC regions (Figure 4D). These results provide evidence that host BC-1 daughter cells give rise to themselves, transitory BC-2 and IC-2 lineages, and IC-1 and S cell populations at bladder augment sites; however, host IC-1 cells do not serve as progenitors.

De Novo S Cell Formation at Bladder Augment Sites Depends on IC-1 Progenitors Derived from Host KRT5$^+$ BC-1 Cells

Next, we sought to understand whether BC-1 daughter cells in the implant regions give rise directly to S cells or indirectly via a UP$^+$ intermediary lineage such as IC-1. To distinguish between these two possibilities, we performed Tm induction on *Upk2*^{iCreERT2};mTmG mice between weeks 4 and 5 after SIS scaffold implantation and harvested bladders for IHC analysis at 8 weeks post-op. This strategy allowed us to lineage trace the progeny of UP$^+$ populations (IC-1, IC-2) present in the graft site at this time point, which had been derived from KRT5$^+$ BC-1 cell daughters as demonstrated in Figure 4B. We predicted two possible experimental outcomes. If BC-1 cell progeny directly differentiate into S cells, we would expect to observe GFP labeling only in the UP$^+$ IC-1 population at 8 weeks post-op. In the event that BC-1 cells in the neotissues first differentiate into IC-1 cells, which then serve as S cell progenitors, we would predict GFP labeling to occur in both IC-1 cells and their S cell descendants. Indeed, our results revealed GFP expression throughout IC-1 and S cells (Figure 4F), suggesting the latter outcome. In addition, we also observed GFP-labeled P63$^+$ IC-1 cells putatively dividing and giving rise to S cells in implant regions. These data provide evidence that host BC-1 daughter cells form S cells indirectly through IC-1 intermediates during repair of surgical defects.

De Novo S Cell Formation during Regeneration of Focal Mucosal Defects Is Dependent on Both Host BC-1 and IC-1 Progenitors

Fate-mapping experiments were then performed in Tm-induced *Krt5*^{CreERT2};mTmG and *Upk2*^{iCreERT2};mTmG mice to discern whether BC-1 or IC-1 cells serve as urothelial progenitors during healing of mucosal defects. Three weeks following injury, IHC analyses of *Krt5*^{CreERT2};mTmG bladders demonstrated GFP expression in both BC-1 and IC-1 cell types within neotissues (Figure 5A) while 23% ± 6% of the S cell population was GFP$^+$ (Figure 5C). Parallel evaluations of *Upk2*^{iCreERT2};mTmG bladders 3 weeks after resection revealed that 56% ± 15% of S cells expressed GFP in the neoepithelium (Figures 5B and 5C). However, there was no significant difference in the percentage of GFP$^+$ S cells detected in comparison with levels achieved in *Krt5*^{CreERT2};mTmG mice (Figure 5C). In addition, GFP$^+$ IC-1 cells were also observed in the regenerated urothelium of *Upk2*^{iCreERT2};mTmG mice (Figure 5B). As expected, inspection of NRC regions at 3 weeks post-op revealed GFP expression concentrated in host BC-1 cells of *Krt5*^{CreERT2};mTmG mice (Figure 5A), while host IC-1 and S cells exhibited GFP labeling in the *Upk2*^{iCreERT2};mTmG strain (Figure 5B). These outcomes demonstrate that both host BC-1 and IC-1 cells contribute to *de novo* urothelial formation during mucosal repair, in contrast to acellular graft remodeling whereby only BC-1 cells serve as urothelial progenitors. Importantly, the ability of both host BC-1 and IC-1 cells to serve as S cell progenitors in the focal mucosal resection model illustrates that linear and nonlinear sequences of urothelial regeneration can occur concurrently in response to this type of injury.

Putative Regulators of Urothelial Differentiation Are Modulated during Repair of Surgical Defects

The retinoic acid (RA) signaling axis is regulated by cyclophosphamide (CPP)-induced injury to the adult bladder and has been demonstrated as a significant driver of urothelial regenerative processes (Gandhi et al., 2013).

arrows denote BC-2 cells (KRT5$^+$P63$^-$UP$^-$KRT20$^-$), yellow arrows denote IC-1 cells (KRT5$^-$P63$^+$UP$^+$KRT20$^-$), purple arrows denote IC-2 cells (KRT5$^-$P63$^-$UP$^+$KRT20$^-$), and white arrows denote S cells (KRT5$^-$P63$^-$UP$^+$KRT20$^+$). Scale bars represent 1 mm (column 1), 500 μm (column 2), and 200 μm (columns 3–6).

(B) Histomorphometric evaluations of urothelial subpopulations in NSC as well as neotissues and corresponding NRC regions following 3 days, 1 week, and 3 weeks post-op. Means ± SD. *$p < 0.05$ in comparison with respective 3-day time point as determined by Wilcoxon signed-rank test.

(C) Histomorphometric evaluations of Ki67$^+$ cells in specimens described in (B). Means ± SD.

Data in all panels were acquired from n = 3 animals per experimental group with n = 3 sections per animal analyzed for neotissue, NRC, and NSC evaluations. See also Figure S1.

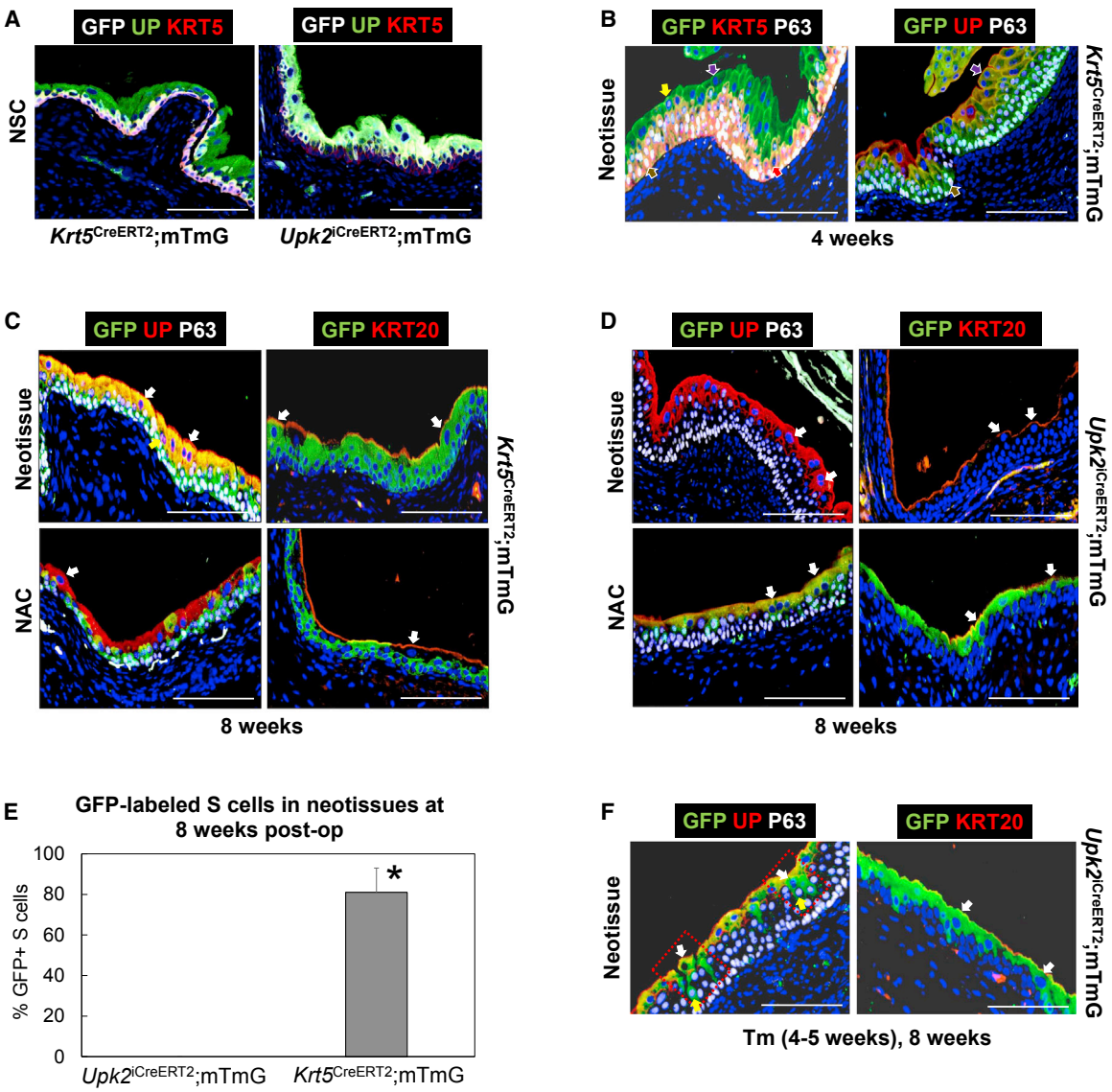

Figure 4. Fate-Mapping Analyses of Urothelial Subpopulations during Regeneration of SIS Graft Sites

(A) Bladder sections from *Krt5*^{CreERT2};mTmG and *Upk2*^{iCreERT2};mTmG nonsurgical control (NSC) mice following Tm induction, demonstrating restricted GFP expression in KRT5- and UP-positive cell layers, respectively.

(B) SIS implant areas in Tm-induced *Krt5*^{CreERT2};mTmG mice at 4 weeks post-op, demonstrating GFP expression in *de novo* BC-1, BC-2, and IC-2 cell populations.

(C) SIS graft sites and nonaugmented control (NAC) regions from Tm-induced *Krt5*^{CreERT2};mTmG mice at 8 weeks post-op demonstrating GFP expression in *de novo* BC-1, IC-1, and S cell populations in neotissues and GFP^{+} host BC-1 cells in NAC.

(D) SIS graft sites and NAC regions in *Upk2*^{iCreERT2};mTmG mice at 8 weeks post-op showing no GFP expression in *de novo* urothelium in neotissues and GFP^{+} IC-1 and S cells in NAC.

(E) Quantitation of GFP^{+} S cells in neotissues present in augmented bladders of Tm-induced *Krt5*^{CreERT2};mTmG and *Upk2*^{iCreERT2};mTmG mice following 8 weeks post-op. Means ± SD. *$p < 0.05$ in comparison with *Upk2*^{iCreERT2};mTmG group as determined by Wilcoxon signed-rank test.

(F) SIS graft regions in *Upk2*^{iCreERT2};mTmG mice at 8 weeks post-op, which were induced by Tm between weeks 4 and 5 following bladder augmentation. *De novo* urothelium demonstrated GFP expression in IC-1 and S cells. Boxed regions demonstrate dividing IC-1 cells giving rise to S cells.

For (A)–(D) and (F), respective marker expression following IHC evaluations is displayed in red, green, or pink (Cy3, FITC, Cy5 labeling), and blue denotes DAPI nuclear counterstain. In some cases, Cy5 labeling was false colored to white. Brown arrows denote BC-1 cells

(legend continued on next page)

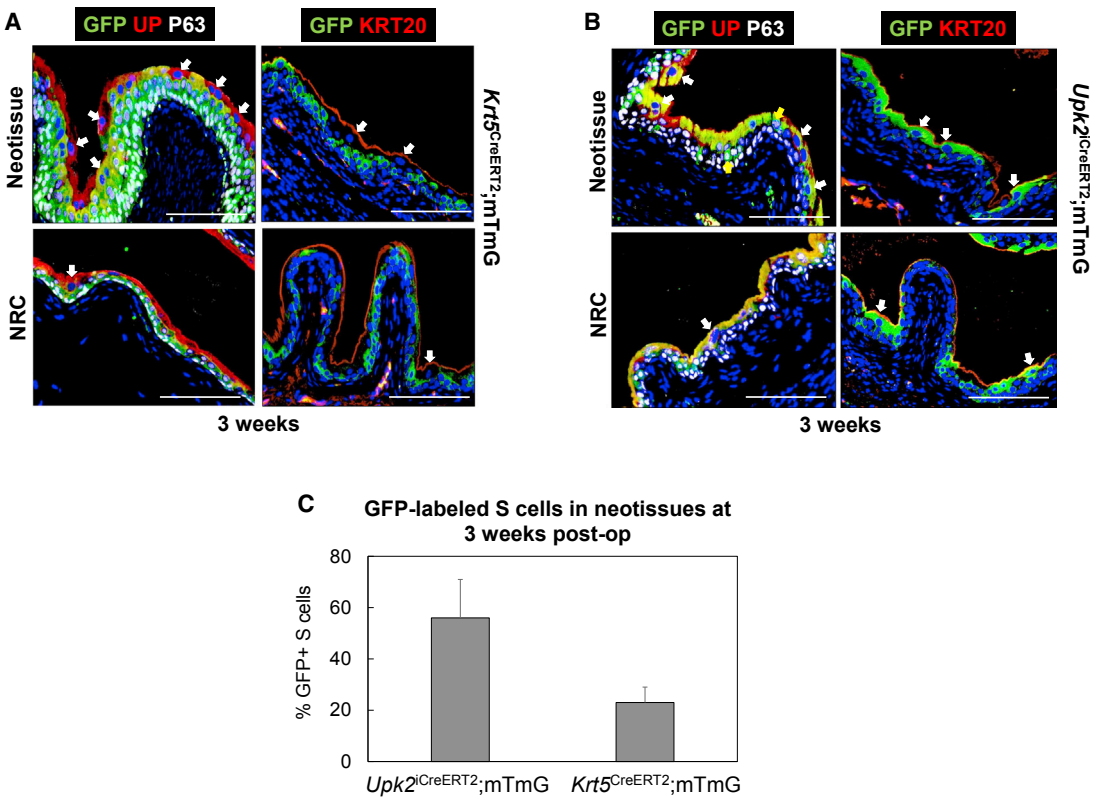

Figure 5. Lineage-Tracing Analyses of Urothelial Subpopulations during Regeneration Focal Mucosal Defects

(A) Sites of mucosal resection and NRC regions in Tm-induced *Krt5*^{CreERT2};mTmG mice at 3 weeks post-op revealing GFP expression in *de novo* BC-1, IC-1, and subsets of S cells in neotissues as well as GFP^{+} host BC-1 cells in NRC.

(B) Sites of mucosal resection and NRC areas in Tm-induced *Upk2*^{iCreERT2};mTmG mice at 3 weeks post-op revealing GFP expression in *de novo* IC-1, and S cell fractions in neotissues as well as GFP^{+} host IC-1 and S in NRC.

(C) Quantitation of GFP^{+} S cells in neotissues present in resected bladders of Tm-induced *Krt5*^{CreERT2};mTmG and *Upk2*^{iCreERT2};mTmG mice following 3 weeks post-op. Means ± SD.

For (A) and (B), respective marker expression following IHC evaluations is displayed in red, green, or pink (Cy3, FITC, Cy5 labeling), and blue denotes DAPI nuclear counterstain. In some cases, Cy5 labeling was false colored to white. Yellow arrows denote IC-1 cells (KRT5^{-}P63^{+}UP^{+}KRT20^{-}) and white arrows denote S cells (KRT5^{-}P63^{-}UP^{+}KRT20^{+}). For all panels, data were acquired from n = 3 animals per experimental group with n = 3 sections per animal analyzed for neotissue and NRC evaluations. Scale bars represent 200 μm (A and B).

However, it is unclear whether this pathway is responsive to surgical injury and, if so, what are the kinetics and distribution of its signaling components within defect sites across various stages of wound healing. To address this, we analyzed the RA pathway component, retinaldehyde dehydrogenase 2 (RALDH2) in WT murine bladders following augmentation cystoplasty and mucosal resection. RALDH2 is an enzyme required for RA synthesis, which is localized to the suburothelial mesenchyme and provides a putative source of RA necessary to drive RA-dependent differentiation of IC-1 cells toward S cells following CPP-induced injury (Gandhi et al., 2013). In comparison with NSC as well as NAC and NRC regions, IHC analysis of RALDH2 protein expression demonstrated a transient peak in the regenerating suburothelial mesenchyme at 1 and 4 weeks following mucosal resection and bladder augmentation with SIS grafts, respectively (Figure 6). Since this trend coincided with the earliest time

(KRT5^{+}P63^{+}UP^{-}KRT20^{-}), red arrows denote BC-2 cells (KRT5^{+}P63^{-}UP^{-}KRT20^{-}), yellow arrows denote IC-1 cells (KRT5^{-}P63^{+}UP^{+}KRT20^{-}), purple arrows denote IC-2 cells (KRT5^{-}P63^{-}UP^{+}KRT20^{-}), and white arrows denote S cells (KRT5^{-}P63^{-}UP^{+}KRT20^{+}). For all panels, data were acquired from n = 3–4 animals per experimental group with n = 3 sections per animal analyzed for neotissue, NAC, NSC evaluations. Scale bars represent 200 μm (A–D and F).

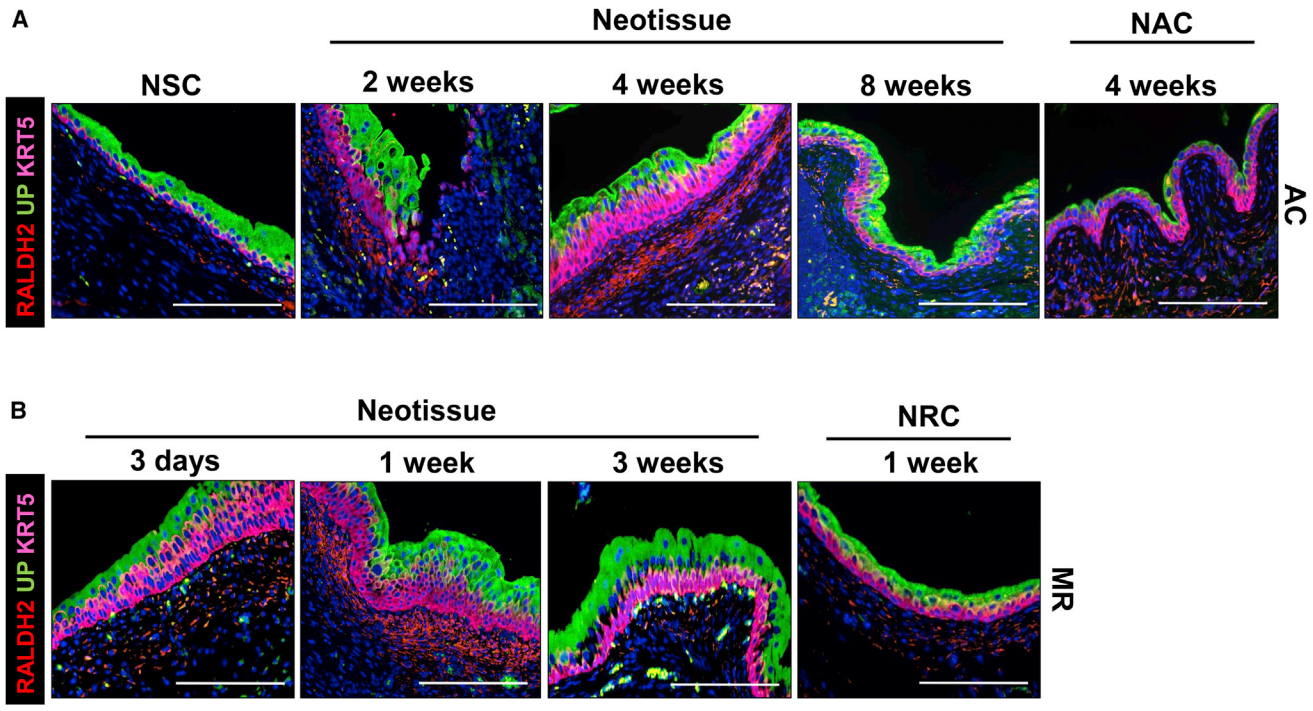

Figure 6. RALDH2 Expression Profiles in Regenerating Neotissues following Augmentation Cystoplasty and Focal Mucosal Resection

(A) IHC evaluations of RALDH2, UP, and KRT5 expression in nonsurgical controls (NSC), SIS graft regions following 2, 4, and 8 weeks post-op, and NAC regions at 4 weeks post repair.

(B) Parallel analysis of markers detailed in (A) during remodeling of mucosal defect sites at 3 days, 1 week, and 3 weeks following injury as well as NRC regions at 1 week post-op. Peak RALDH2 expression is detected in the suburothelial mesenchyme at 1 and 4 weeks following mucosal resection and bladder augmentation, respectively.

For all panels, respective marker expression is displayed in red, green, or pink (Cy3, FITC, Cy5 labeling), and blue denotes DAPI nuclear counterstain. AC, augmentation cystoplasty; MR, mucosal resection. Representative data from n = 3 NSC animals and n = 3–5 mice per time point for neotissues in AC and MR groups as well as NAC and NRC regions. Three sections were evaluated for each animal replicate per group. Scale bars represent 200 μm.

points at which S cells were first detected in neotissues, upregulation of RA synthesis may be important for IC-1 specification toward an S cell phenotype during surgical defect healing, although additional investigation is needed to confirm this notion.

DISCUSSION

In the present study, we have characterized the cellular basis of urothelial regenerative responses to various modes of surgical bladder injury, including acellular graft implantation and focal mucosal resection. We have shown using fate-mapping techniques that host BC-1 cells are the sole progenitors of *de novo* urothelial formation at graft sites in which they form themselves, IC-1, and S cells in a linear sequence as well as transitory BC-2 and IC-2 cell populations. By comparison, repair of mucosal defects following focal resection not only involves this process, but host IC-1 cells also serve as S cell progenitors in this setting. In this context, we observed that linear and nonlinear sequences of urothelial regeneration are not mutually exclusive. It is currently unknown why the pattern of urothelial regeneration differs in these two injury models. Previous reports of host bladder responses to bacterial infection and protamine sulfate treatment have shown positive correlations between levels of injury-induced inflammation and differential activation of progenitor cell populations in the urothelium (Mysorekar et al., 2009). Specifically, bromodeoxyuridine pulse-chase experiments have demonstrated that BC-1 cell daughters selectively contribute to S cell formation following inflammatory bacterial infection, while protamine sulfate-induced urothelial damage results in minimal inflammation and promotes S cell differentiation through IC-1 progeny, in contrast to BC-1 cell descendants (Mysorekar et al., 2009). In our experiments,

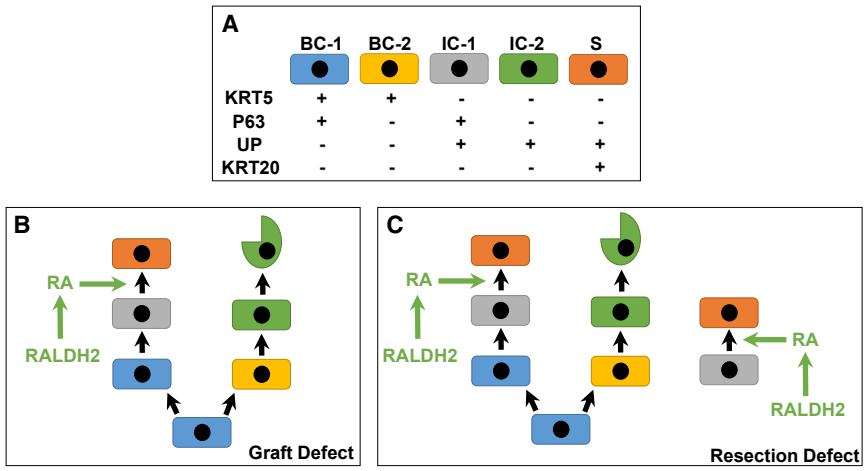

Figure 7. Model of Urothelial Lineage Hierarchy and RA Signaling during Regeneration of Surgical Defects

(A) Urothelial subpopulations and associated markers in normal and regenerating tissues.

(B) Following augmentation cystoplasty, host BC-1 cells proliferate at defect sites and at early stages of defect repair give rise to BC-2 cells. BC-2 cells then differentiate into IC-2 cells, which then undergo exfoliation. At latter phases of remodeling, BC-1 cells undergo IC-1 differentiation. Subsequently, upregulation of RALDH2 expression in the suburothelial mesenchyme leads to RA synthesis, which promotes IC-1 differentiation toward an S cell phenotype, leading to restoration of urothelial barrier function.

(C) During repair of mucosal defects, the process described in (A) occurs. In parallel, host IC-1 cells invade the remodeling tissue and their progeny undergo S cell differentiation in response to RA.

we routinely observed inflammatory mononuclear cells throughout the regenerating mucosa over the course of the 8-week scaffold implantation period. However, a sharp decline in this population was noted at sites of focal mucosal resection between 1 and 3 weeks following injury, a period during which host IC-1 cells give rise to the majority of S cells. Therefore, the persistent host inflammatory response at bladder augment sites may serve to inhibit the ability of host IC-1 cell daughters to participate in urothelial regenerative processes and may explain why host BC-1 cells were observed as the primary urothelial progenitor population in this setting. Future experiments will focus on the role of inflammatory mediators in mediating urothelial progenitor hierarchy.

Our data demonstrate that host BC-1 cells temporally bifurcate along two different lineage pathways during repair of surgical defect sites. The first mode of BC-1 specification occurs in the early stages of the regenerative process and involves production of transient BC-2 cells that putatively differentiate into IC-2 cells, which are subsequently exfoliated into the lumen as defect consolidation proceeds. The second type of progression commences during the latter stages of repair and consists of differentiation of host BC-1 cell daughters into IC-1 cells, which then give rise to S cells allowing for restoration of urothelial integrity. The function of transitory BC-2 and IC-2 phenotypes during urothelial regeneration is currently unknown and deserves further study. However, one possible explanation may be that these cell types serve as a temporary "scab-like" layer that shields the remodeling tissue from urinary toxins, allowing *de novo* IC-1 and S cell formation to occur.

Signaling mechanisms that facilitate urothelial regeneration following bladder reconstruction are not well defined. Based on our findings that the RA signaling component, RALDH2, is differentially modulated along various stages of bladder repair, we propose a model (Figure 7) wherein upregulation of RA synthesis by RALDH2 in the suburothelial mesenchyme drives newly formed IC-1 cells to differentiate into S cells in an RA-dependent manner in order to restore native urothelial architecture. In the case of focal mucosal resection, host IC-1 cells also migrate and proliferate into the defect site in parallel and serve S cell progenitors in response to RA. Elucidation of the role of RA signaling in cell fate specification during surgical bladder repair is ongoing in our laboratory.

In conclusion, our study demonstrates that the mode of surgical injury influences the source of urothelial progenitors utilized during bladder repair. In the case of augmentation cystoplasty with acellular grafts, BC-1 cell daughters represent the major progenitor pool responsible for mediating *de novo* urothelial formation at scaffold implantation sites, while focal mucosal resection activates both BC-1 and IC-1 cell progeny to reconstitute the native urothelium following injury. Taken together, our results show that the pattern of urothelial regeneration can occur exclusively through a linear progression or via both linear and nonlinear pathways concurrently, depending on the type of surgical injury employed. In addition, modulation of the RA signaling axis occurs during surgical defect repair and may influence urothelial progenitor specification. Determination of how urothelial injury responses are regulated at the molecular level in healthy and diseased tissues following surgical bladder

damage may lead to the development of tissue engineering advances.

EXPERIMENTAL PROCEDURES

Mouse Strains and Genotyping

All animal studies were approved by the Boston Children's Hospital Animal Care and Use Committee prior to experimentation and performed under protocol 14-08-2771R. WT mice (Swiss Webster, 6–8 weeks of age) were obtained from Charles River Laboratories (Wilmington, MA). Transgenic mouse strains (6–8 weeks of age) from Jackson Laboratories (Bar Harbor, ME) were utilized and included FVB.Cg-Tg(*Krt5*-cre/ERT2)2Ipc/JeldJ mice (stock no. 018394, designated *Krt5*^{CreERT2} mice), which express Tm-inducible Cre recombinase under the direction of the bovine *Krt5* promoter/enhancer regions (Indra et al., 1999), B6; CBA-Tg(*Upk2*-icre/ERT2)1Ccc/J mice (stock no. 024768, designated *Upk2*^{iCreERT2} mice), which express Tm-inducible Cre recombinase under the control of mouse uroplakin 2 promoter (Shen et al., 2012); and Gt(ROSA)26Sortm4(ACTB-*tdTomato*,-*eGfp*)Luo/J mice (stock no. 007676, designated mTmG mice). *Krt5*^{CreERT2} and *Upk2*^{iCreERT2} mice were independently crossed with mTmG mice to generate *Krt5*^{CreERT2};mTmG and *Upk2*^{iCreERT2};mTmG strains. In these lines, membrane-bound GFP is expressed in cells that undergo Cre-dependent recombination, and membrane-bound Tomato is expressed in cells where recombination has not taken place (Muzumdar et al., 2007). Genotyping was performed with tail clipping under isoflurane anesthesia using appropriate probes by Transnetyx (Cordova, TN). For all lineage-tracing studies, *Krt5*^{CreERT2};mTmG and *Upk2*^{iCreERT2};mTmG mouse strains were injected intraperitoneally with 5 mg of Tm per 30 g body weight (Sigma-Aldrich, St. Louis, MO) daily for 3 consecutive days and maintained for at least 7 days thereafter before commencement of surgical procedures or harvesting as NSC to allow for genetic recombination to occur, unless otherwise noted.

Surgical Models

Urothelial regeneration was characterized in WT and transgenic mouse strains in two independent surgical injury models including augmentation cystoplasty (Figure 1A) with SIS scaffolds (Biodesign 4-Layer Tissue Graft, Cook Medical, Bloomington, IN) (Mauney et al., 2011) as well as focal mucosal resection (Figure 1B). In both surgical procedures, animals were anesthetized using isoflurane inhalation and then shaved to expose the surgical site. All surgeries were performed under 10× microscopic magnification. A low midline laparotomy incision was made and the underlying tissue (rectus muscle and peritoneum) was dissected to expose the bladder. For bladder augmentation, the bladder dome was opened and a 5-mm circular SIS patch was sutured into the bladder wall using 8-0 polyglactin (Vicryl) continuous suture. In addition, four polypropylene sutures were used to mark the perimeter of the anastomosis. A watertight seal was confirmed by filling the bladder with sterile saline via instillation through a 30-gauge hypodermic needle. For mucosal resection, two polypropylene sutures were placed into the exposed bladder to demarcate the injury site, and a midline incision was performed. The urothelium and underlying submucosa were then resected from two-thirds of the bladder surface area using micro-forceps, leaving the trigone and ureteral orifices intact. Bladder closure was achieved with 8-0 polyglactin (Vicryl) continuous sutures. Following defect creation in both models, wound and skin closure were performed and local injection of bupivacaine into the rectus muscle and subcutaneous tissue was administered. Bladders receiving SIS implants were harvested at 2, 4, and 8 weeks post-op while those undergoing mucosal resection were euthanized at 12 hr, 3 days, 1 week, and 3 weeks post injury. Tissue specimens were then subjected to histological, IHC, and histomorphometric analyses detailed below.

Histological, IHC, and Histomorphometric Analyses

Following scheduled euthanasia by CO_2 inhalation, bladders from experimental groups were formalin-fixed, dehydrated in graded alcohols, and embedded in paraffin. Sections (5 μm) were cut and stained with Masson's trichrome (MTS) using standard methods. Parallel specimens were analyzed for IHC assessments utilizing primary antibodies to select antigens including KRT5 (chicken immunoglobulin G [IgG], 1:500 dilution, cat. no. 905901, BioLegend, San Diego, CA); P63 (rabbit IgG, 1:200 dilution, cat. no. GTX102425, Genetex, Irvine, CA); UP 3A (goat IgG, 1:200 dilution, cat. no. sc-15186, Santa Cruz Biotechnology, Santa Cruz, CA); KRT20 (mouse IgG, 1:50 dilution, cat. no. M7019, Dako, Carpinteria, CA); GFP (rabbit IgG, 1:1,000 dilution, cat. no. 600-401-215 and goat IgG, 1:200 dilution, cat. no. 600-101-215, Rockland, Limerick, PA); KI67 (rabbit IgG, 1:200 dilution, cat. no. ab15580, Abcam, Cambridge, MA); RALDH2 (rabbit IgG, 1:500 dilution, cat. no. HPA010022, Sigma-Aldrich); and cleaved caspase-3 (rabbit IgG, 1:200 dilution, cat. no. AB3623, Millipore, Billerica, MA). For IHC evaluations, sections were first deparaffinized in xylene and then rehydrated in graded alcohols, subjected to antigen retrieval in 10 mM sodium citrate buffer (pH 6.0), and incubated for 1 hr in blocking buffer consisting of PBS with 5% fetal bovine serum, 1% BSA, and 0.3% Triton X-100 for 1 hr at room temperature. Specimens were incubated with primary antibodies at specified dilutions overnight at 4°C and subsequently washed in PBS at room temperature. Sections were then incubated for 1 hr at room temperature with species-matched Cy3, Cy5, or fluorescein isothiocyanate (FITC)-conjugated secondary antibodies (Millipore). Following specimen washing with PBS, nuclei were counterstained with DAPI. Sample visualization was performed with an Axioplan-2 microscope (Carl Zeiss MicroImaging, Thornwood, NY) and representative fields were acquired with Axiovision software (version 4.8). Histomorphometric evaluations (n = 3–4 animals per group) were performed on three independent microscopic fields (20× magnification) using published methods (Algarrahi et al., 2015) to quantify urothelial subpopulations in experimental cohorts.

Statistical Analyses

All quantitation was carried out on at least three independent animal replicates per group. Statistical analyses of quantitative data in control (NSC, NAC, NRC) and experimental (neotissues) groups was performed with R statistical software v.3.0.2 (R Core Team, R Foundation for Statistical Computing, Vienna, Austria; http://www/R-project.org). The percentages of urothelial subpopulations

in neotissues and respective controls were compared across experimental time points using the Kruskal-Wallis statistical test. In addition, the percentages of $Ki67^{+}$ urothelial subpopulations in neotissues and respective controls were analyzed similarly. For two-group comparisons, statistical significance was determined using a Wilcoxon signed-rank test, considering a value of $p < 0.05$ as significant.

SUPPLEMENTAL INFORMATION

Supplemental Information includes one figure and can be found with this article online at https://doi.org/10.1016/j.stemcr.2017.10.025.

AUTHOR CONTRIBUTIONS

F.-M.S., C.S., R.A., and J.R.M. conceived and designed the experiments and analyzed data. F.-M.S., K.A., and X.Y. performed experiments and analyzed data. D.F., A.S., X.Y., and K.C. analyzed and processed data. T.L. and S.L. performed statistical analyses. F.-M.S. and J.R.M. wrote the paper. All authors edited the paper. J.R.M. coordinated and supervised all aspects of the study.

ACKNOWLEDGMENTS

This research was supported through the vision and generosity of the Rainmaker Group in honor of Dr. Alan Retik, MD. This study was also supported by a postdoctoral research grant from the Max Kade Foundation to F.M.S. The authors thank Dr. Cathy Mendelsohn at Columbia University for helpful discussions and critical review of the manuscript.

Received: April 11, 2017
Revised: October 26, 2017
Accepted: October 27, 2017
Published: November 22, 2017

REFERENCES

Abraham, S.N., and Miao, Y. (2015). The nature of immune responses to urinary tract infections. Nat. Rev. Immunol. *15*, 655–663.

Algarrahi, K., Franck, D., Ghezzi, C.E., Cristofaro, V., Yang, X., Sullivan, M.P., Chung, Y.G., Affas, S., Jennings, R., Kaplan, D.L., et al. (2015). Acellular bi-layer silk fibroin scaffolds support functional tissue regeneration in a rat model of onlay esophagoplasty. Biomaterials *53*, 149–159.

Balsara, Z.R., and Li, X. (2017). Sleeping beauty: awakening urothelium from its slumber. Am. J. Physiol. Renal Physiol. *312*, F732–F743.

Gandhi, D., Molotkov, A., Batourina, E., Schneider, K., Dan, H., Reiley, M., Laufer, E., Metzger, D., Liang, F., Liao, Y., et al. (2013). Retinoid signaling in progenitors controls specification and regeneration of the urothelium. Dev. Cell *26*, 469–482.

Indra, A.K., Warot, X., Brocard, J., Bornert, J.M., Xiao, J.H., Chambon, P., and Metzger, D. (1999). Temporally-controlled site-specific mutagenesis in the basal layer of the epidermis: comparison of the recombinase activity of the tamoxifen-inducible Cre-ER(T) and Cre-ER(T2) recombinases. Nucleic Acids Res. *27*, 4324–4327.

Khandelwal, P., Abraham, S.N., and Apodaca, G. (2009). Cell biology and physiology of the uroepithelium. Am. J. Physiol. Renal Physiol. *297*, F1477–F1501.

Kullmann, F.A., Clayton, D.R., Ruiz, W.G., Wolf-Johnston, A., Gauthier, C., Kanai, A., Birder, L.A., and Apodaca, G. (2017). Urothelial proliferation and regeneration after spinal cord injury. Am. J. Physiol. Renal Physiol. *313*, F85–F102.

Mauney, J.R., Cannon, G.M., Lovett, M.L., Gong, E.M., Di Vizio, D., Gomez, P., Kaplan, D.L., Adam, R.M., and Estrada, C.R. (2011). Evaluation of gel spun silk-based biomaterials in a murine model of bladder augmentation. Biomaterials *32*, 808–818.

Muzumdar, M.D., Tasic, B., Miyamichi, K., Li, L., and Luo, L. (2007). A global double-fluorescent Cre reporter mouse. Genesis *45*, 593–605.

Mysorekar, I.U., Isaacson-Schmid, M., Walker, J.N., Mills, J.C., and Hultgren, S.J. (2009). Bone morphogenetic protein 4 signaling regulates epithelial renewal in the urinary tract in response to uropathogenic infection. Cell Host Microbe *5*, 463–475.

Papafotiou, G., Paraskevopoulou, V., Vasilaki, E., Kanaki, Z., Paschalidis, N., and Klinakis, A. (2016). KRT14 marks a subpopulation of bladder basal cells with pivotal role in regeneration and tumorigenesis. Nat. Commun. *7*, 11914.

Richards, K.A., Smith, N.D., and Steinberg, G.D. (2014). The importance of transurethral resection of bladder tumor in the management of nonmuscle invasive bladder cancer: a systematic review of novel technologies. J. Urol. *191*, 1655–1664.

Schaefer, M., Kaiser, A., Stehr, M., and Beyer, H.J. (2013). Bladder augmentation with small intestinal submucosa leads to unsatisfactory long-term results. J. Pediatr. Urol. *9*, 878–883.

Shen, T.H., Gladoun, N., Castillo-Martin, M., Bonal, D., Domingo-Domenech, J., Charytonowicz, D., and Cordon-Cardo, C. (2012). A BAC-based transgenic mouse specifically expresses an inducible Cre in the urothelium. PLoS One *7*, e35243.

Shin, K., Lee, J., Guo, N., Kim, J., Lim, A., Qu, L., Mysorekar, I.U., and Beachy, P.A. (2011). Hedgehog/Wnt feedback supports regenerative proliferation of epithelial stem cells in bladder. Nature *472*, 110–114.

Veeratterapillay, R., Thorpe, A.C., and Harding, C. (2013). Augmentation cystoplasty: contemporary indications, techniques and complications. Indian J. Urol. *29*, 322–327.

Wu, X.R., Kong, X.P., Pellicer, A., Kreibich, G., and Sun, T.T. (2009). Uroplakins in urothelial biology, function, and disease. Kidney Int. *75*, 1153–1165.

Zhang, F., and Liao, L. (2014). Tissue engineered cystoplasty augmentation for treatment of neurogenic bladder using small intestinal submucosa: an exploratory study. J. Urol. *192*, 544–550.